Torque Ripple Minimization of PMSM Based on Robust ILC Via Adaptive Sliding Mode Control

Jing Liu, *Student Member, IEEE*, Hongwen Li, *Member, IEEE*, and Yongting Deng, *Member, IEEE*

***Abstract*—Torque ripples due to cogging torque, current measurement errors, and flux harmonics restrict the application of the permanent magnet synchronous motor (PMSM) that has a high-precision requirement. The torque pulsation varies periodically along with the rotor position, and it results in speed ripples, which further degrade the performance of the PMSM servo system. Iterative learning control (ILC), in parallel with the classical proportional integral (PI) controller (i.e., PI-ILC), is a conventional method to suppress the torque ripples. However, it is sensitive to the system uncertainties and external disturbances, i.e., it is paralyzed to nonperiodic disturbances. Therefore, this paper proposes a robust ILC scheme achieved by an adaptive sliding mode control (SMC) technique to further reduce the torque ripples and improve the antidisturbance ability of the servo system. ILC is employed to reduce the periodic torque ripples and the SMC is used to guarantee fast response and strong robustness. An adaptive algorithm is utilized to estimate the system lumped disturbances, including parameter variations and external disturbances. The estimated value is utilized to compensate the robust ILC speed controller in order to eliminate the effects of the disturbance, and it can suppress the sliding mode chattering phenomenon simultaneously. Experiments were carried out on a digital signal processor-field programmable gate array based platform. The obtained experimental results demonstrate that the robust ILC scheme has an improved performance with minimized torque ripples and it exhibits a satisfactory antidisturbance performance compared to the PI-ILC method.**

***Index Terms*—Adaptive algorithm, iterative learning control (ILC), motor drives, permanent magnet synchronous motor (PMSM), robust, sliding mode control (SMC), torque ripple.**

I. Introduction

PERMANENT magnet synchronous motor (PMSM) is an appealing candidate for many high-precision applications, because of its attractive characteristics in terms of efficiency, power density, torque-to-inertia ratio, reliability, etc. However, inherent torque ripples in the PMSM are encountered in many industrial applications. These torque ripples induce periodic oscillations in the motor speed. These speed oscillations usually lead to a degradation of the servo system performance and further cause undesirable mechanical vibrations at low speed and an acoustic noise at high speed [1].

Usually, the periodic torque ripples can be attributed to various sources, e.g., flux harmonics, cogging torque, current measurement errors, and phase unbalancing [2], [3]. Several methods have been proposed to deal with the issue of pulsating torque. Generally, these methods can be categorized into two types. The first type consists of techniques that focus on the improvement of motor design, such as skewing the slot or magnet, ensuring fractional number of slots per pole, improving the winding distribution, etc. [4]. Optimization of motor design is a natural and effective approach to weaken the torque ripple phenomenon. However, the applicability of these techniques is limited to newly developed motors, and they can result in a further complicated realization and higher manufacturing cost. The second type includes active control techniques, which modify the input current or voltage, using control methods for the attenuation of torque ripples. As the controller is a necessary part of the PMSM servo system, the active control technique requires no additional hardware. Moreover, the active control technique can be easily matched to most types of motor machines.

Therefore, this paper focuses on the second type that uses active control techniques to reduce the torque ripples. In previous works, active control techniques are used to store preprogrammed current in a look-up table to cancel torque ripples at specific positions, which are open-loop compensation approach [5]–[7]. However, in such a method, sufficiently accurate information of the PMSM parameters, in particular, preknowledge of the relationships between the torque ripples and stator excitation currents, must be obtained. A small error or variation in the parameters can lead to even higher torque ripples due to the open-loop feed-forward control.

Thereafter, closed-loop control algorithms have been proposed in [8]–[19]. These control schemes are implemented either in speed or current (torque) loops. In torque control schemes, a popular method is to regulate the torque using online estimated torque based on the electrical subsystem variables only. Various algorithms have been proposed for instantaneous torque estimation [4], [20]–[22]. But, on the other hand, this approach can be used only for those torque ripple components that are observable from the electrical subsystem; ripples due to mechanical parts (e.g., cogging torque and load oscillations) cannot be estimated from the electrical subsystem variables, and therefore are uncontrollable. An alternative technique is to use

Manuscript received December 21, 2016; revised April 4, 2017; accepted May 23, 2017. Date of publication June 1, 2017; date of current version January 3, 2018. This work was supported in part by the National Natural Science Foundation of China under Grant 11603024, and in part by the Third Phase of Innovation Project of Changchun Institute of Optics, Fine Mechanics, and Physics, Chinese Academy of Science under Grant 065X32CN60. Recommended for publication by Associate Editor I. Slama-Belkhodja. *(Corresponding author: Yongting Deng.)*

The authors are with the Changchun Institute of Optics, Fine Mechanics and Physics, Chinese Academy of Science, Changchun 130033, China (e-mail: nuaaliujing@163.com; lihongwen1970@yahoo.com; dyt0612@163.com).

Color versions of one or more of the figures in this paper are available online at http://ieeexplore.ieee.org.

Digital Object Identifier 10.1109/TPEL.2017.2711098

a torque transducer, which could increase the cost of the drive system significantly.

As all possible sources of torque ripples are observable from the rotor speed, methods that rely on a closed-loop speed regulator can accomplish the same objective indirectly. Furthermore, these methods have potential for complete torque ripple minimization. Iterative learning control (ILC) is an approach to improve the performance of a system that executes repetitively and periodically over a fixed time interval, by learning from previous executions (trials, iterations, and passes) [23]. Since torque ripple reduction can be regarded as a periodic disturbance rejection problem, the ILC technique naturally fits this goal as presented in [1], [12], and [24]–[27]. Conventionally, the speed controller relies on the ILC in parallel with the proportional integral (PI) control to compensate the reference current, and it achieves impressive torque ripple depression. However, the scheme that combines PI and ILC is paralyzed to a nonperiodic object. It is sensitive to the uncertainty of the system parameters, and the antidisturbance ability is weak. Therefore, robustness of the system should be considered, when the ILC method is used to reduce torque ripples.

Sliding mode control (SMC) is a popular nonlinear control to handle disturbances, and it exhibits advantages such as quick response, strong robustness, and simple implementation [28], [29]. Therefore, to deal with the periodic torque ripples and the nonperiodic disturbance of the system, a robust ILC controller via SMC is developed. Conventionally, in SMC the switching gain should be set large enough to offset the system disturbance in order to guarantee strong robustness and stability of the system, i.e., the minimum switching gain must increase along with the increasing system disturbance. However, in practice, the upper bound of the system disturbance is difficult to determine; meanwhile, owing to the switching function in the control law, the large switching gain will lead to the occurrence of high-frequency sliding mode chattering. To overcome the aforementioned drawbacks, an adaptive algorithm is employed to estimate the lumped system disturbances, including parameter variations and external disturbance. Subsequently, the estimated value is applied to compensate the robust ILC speed controller. This paper presents and validates a robust ILC scheme that synthesizes ILC and adaptive sliding mode technique with the help of the Lyapunov direct method for torque ripple reduction, and it is implemented in the speed loop. The ILC is employed to inhibit the periodic disturbance, i.e., periodic torque ripples. Meanwhile, the adaptive SMC acts as the robust part. The adaptive SMC deals with the system parameter variations and external disturbances, to ensure the global asymptotic stability and to speed up the system response.

This paper is organized as follows. In Section II, the mathematical model of the PMSM is described. Section III briefly analyzes the source of the torque ripples, and the speed ripples induced by the torque ripples are presented. The scheme of a robust ILC via adaptive SMC is explained in Section IV, where the convergence of the output tracking error is also proven using the Lyapunov direct method. In Section V, the implementation of the PMSM drive system is introduced. In Section VI, experiments are implemented to demonstrate the effectiveness of the proposed robust ILC scheme where the experimental results are also derived and discussed. The paper is concluded in Section VII.

II. Mathematical Model of PMSM

Under the assumptions that the PMSM iron core is unsaturated and the eddy currents and hysteresis losses are negligible, the stator $d-q$ axis voltage equations of the PMSM in the synchronous rotating reference frame can be expressed as follows:

$$u_d = Ri_d + \frac{d\lambda_d}{dt} - \omega_e \lambda_q$$
$$u_q = Ri_q + \frac{d\lambda_q}{dt} + \omega_e \lambda_d \tag{1}$$

where $\lambda_d = L_d i_d + \psi_d$ and $\lambda_q = L_q i_q + \psi_q$ are the total flux linkages along the d and q axes, respectively, ψ_d and $\psi_q (\psi_q = 0)$ are the PM flux linkages along the d and q axes, respectively, and ω_e is the electrical angular speed. Furthermore, u_d and u_q are the stator voltages along the d and q axes, respectively, i_d and i_q are the stator currents along the d and q axes, respectively, R is the stator resistance, and L_d and L_q are the stator inductances along the d and q axes, respectively. It has been further assumed that, since the surface-mounted PMSM is nonsalient, L_d and L_q are equal, i.e., $L_d = L_q$.

The equation of PMSM dynamic is

$$J\frac{d\omega_m}{dt} = T_m - T_L - B\omega_m \tag{2}$$

where ω_m is the mechanical angular speed, J is the inertia, T_m is the electromagnetic torque, T_L is the load torque, and B is the frictional coefficient.

Using the method of field-oriented control (FOC) of the PMSM, the *d*-axis current is maintained at zero to maximize the output torque. The electromagnetic torque mathematic model can be expressed as

$$T_m = \frac{3}{2}p\left(\lambda_d i_q - \lambda_q i_d\right) = \frac{3}{2}p\psi_d i_q = K_t i_q \tag{3}$$

where K_t is the torque coefficient and p is the number of pole pairs.

III. Analysis of Torque Ripples

A. Analysis of Torque Ripples

The main causes of torque ripples include cogging torque, flux harmonics, and current measurement errors, and they are briefly analyzed as follows.

Cogging torque is manifested by the tendency of the rotor to align with a number of stable positions, even when the machine is unexcited. It is caused by the interaction between the magnetic flux and stator slots. Until now, no accurate modeling has been available for the cogging torque. According to the analysis presented in [30], the cogging torque can be modeled as a periodic function of the rotor position, which depends on the number of stator slots and rotor pole pairs. It can be suppressed by specific control methods.

Flux harmonics is another main source of torque ripples. Due to the nonsinusoidal flux density distribution in the air gap, the resultant flux linkage between the permanent and stator currents contains harmonics, which appear 3rd, 5th, 7th, 11th ... in the $a-b-c$ frame(triple harmonics are absent in the Y-connected stator windings) [25]. In the $d-q$ frame, the corresponding harmonics appear sixth and at the multiples of the sixth-order harmonics, and they can be expressed as

$$\psi_d(\theta_e) = \psi_{d0} + \psi_{d6}\cos(6\theta_e) + \psi_{d12}\cos(12\theta_e) + \cdots \quad (4)$$

where $\varphi_{d0} = \varphi_f$, in which φ_f is the rotor PM flux linkage. Coefficients φ_{dk} are constants related to the PM flux linkage, and θ_e is the electrical angle.

Combining (3) and (4) yields

$$T_m = T_0 + T_6\cos(6\theta_e) + T_{12}\cos(12\theta_e) + \cdots \quad (5)$$

where T_0, T_6, and T_{12} are the dc component, 6th and 12th harmonic torque magnitudes, respectively. Equation (5) indicates that the 6th and 12th torque harmonics produced mainly due to the nonsinusoidal flux distribution are periodic in nature. Since $\theta_e = 4\theta_m$, the harmonic torque can also be considered as a function of the mechanical angle θ_m.

Current offsets and scaling errors also cause the torque to oscillate at specific frequencies. Stator currents are measured and converted to voltage by current sensors. Furthermore, any voltage fluctuations may affect the measurement error, resulting in a controlled amount of fluctuation. The analysis in [1] showed that the dc offsets in the current measurement give rise to a torque oscillation at the fundamental frequency, and the scaling errors cause the torque to oscillate at twice the fundamental frequency.

These analyses indicate that the electromagnetic torque consists of a fundamental component together with the 1st, 2nd, 6th, 12th harmonic components, etc. The control objective is to suppress these periodic torque ripples via the proposed control method.

B. Speed Ripples Induced by Torque Ripples

The transfer function between the motor mechanical angle speed ω_m and the electromagnetic torque T_m is expressed as

$$\omega_m(s) = \frac{T_m(s) - T_L(s)}{Js + B} \quad (6)$$

where $T_m = f(\psi_d, i_q, \omega_m)$. It can be concluded that the speed will oscillate at the same harmonic frequencies as those of T_m, especially at low operating speeds. In order to reduce the speed ripples, their sources, i.e., the torque ripples, need to be minimized.

IV. Design of Robust ILC Via Adaptive Sliding Mode Control

A. Iterative Learning Control Algorithm

ILC is actually an error-correction algorithm, which is based on a memory that stores the previous controller output data and error information. The iterative learning controller calculates the error $e_k(t)$ between the desired output $y_d(t)$ and the actual system output $y_k(t)$, and computes a new control input $u_{k+1}(t)$,

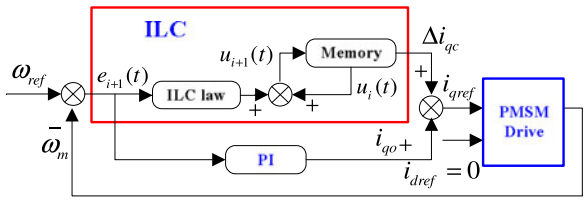

Fig. 1. Block diagram of PI-ILC scheme.

which is stored in the memory for use in the next cycle of operation. The new control input is evaluated based on the criteria that the reduction of $e_k(t)$ is guaranteed by iteration [23].

For a qualitative description of the ILC operation, the following dynamic system is considered:

$$\begin{aligned} \dot{x}(t) &= a_0 x(t) + b_0 u(t) + \delta(t) \\ y(t) &= c_0 x(t) \end{aligned} \quad (7)$$

where a_0 and b_0 are piecewise continuous in t for all $t \in [0, T]$, T is the time period of the desired output, c_0 is differentiable in x and t, and $\delta(t)$ represents the unstructured uncertainties due to state perturbations.

The P-type algorithm is widely used in ILC control as it is simple to implement. Meanwhile, in contrast to the D-type, the differentiation of the speed signal is unnecessary in the P-type algorithm. Hence, noise build-up in the input update caused by the differentiation of speed signal can be avoided. The P-type ILC scheme is expressed as follows:

$$u_{k+1}(t) = u_k(t) + \Gamma(e_k(t)) \quad (8)$$

where k indicates the number of iterations, $u_k(t)$ is the control signal generated from the ILC, $e_k(t)$ is the error signal, and $\Gamma(e_k(t))$ is the learning law.

For convergence of the ILC system, given ξ as the learning gain, the following criterion must hold [1]:

$$\|I - c_0 b_0 \xi\| < 1. \quad (9)$$

The overall block diagram of the conventional PI-ILC method is shown in Fig. 1. i_{qo} is provided by the PI speed controller, and ILC is applied to provide the additional compensation term Δi_{qc} to i_{qo}, to minimize the periodic speed ripples.

B. Robust ILC Design Using the Adaptive Sliding Mode Technique

The underlying robust ILC scheme synthesizes the ILC with adaptive SMC. ILC learns and approaches the unknown state-dependent function and leaves other system uncertainties and external disturbances to be handled by the adaptive SMC. The global asymptotic convergence with respect to iterations is established by the Lyapunov direct method.

According to (2), the PMSM dynamical system is described as follows, where the parameter variations and external disturbances are taken into account

$$\begin{cases} \dot{x}(t) = f(x,t) + bu(t) - r(t) - B(x,t) \\ y(t) = x(t) \end{cases} \quad (10)$$

where the measurable system state $x(t) = \omega_m$. $u(t) = i_{q\mathrm{ref}}$ and $y(t) = \omega_m$ are the control input and system output, respectively. Furthermore, $f(x,t)$ is an unknown state-dependent function to be learned, b is a known constant, $r(t)$ represents the total of external disturbances and parameter variations, and $B(x,t)$ is a known friction torque function.

Before presenting the proposed robust ILC scheme, the following assumptions are first addressed.

Assumption 1: The desired output $\omega_{\mathrm{ref}}(t)$ is differentiable with respect to time t on a finite time interval $[0,T]$, and all the higher order derivatives are available.

Assumption 2: The unknown lumped disturbance variable $r(t)$ is bounded such that $|r(t)| \le l_d, \forall t \in [0,T]$, where l_d is a known constant.

Assumption 3: The initial condition is $e(0) = \dot{e}(0)$ at any iteration $\forall t \in [0,T]$, such that the sliding mode switching surface $S(0) = 0$, where $e(t)$ is the output speed tracking error that is defined as $e(t) = \omega_{\mathrm{ref}}(t) - \omega_m(t)$.

Subsequently, a control law $u(t)$ is designed for the nonlinear system (10), such that the system output ω_m can follow the given reference speed ω_{ref} with prescribed accuracy ε as follows:

$$\forall t \in [0,T], |\omega_{\mathrm{ref}}(t) - \omega_m(t)| \le \varepsilon.$$

Considering the system (10), an integral sliding mode switching surface is defined as follows:

$$S(t) = e(t) + c\int_0^t e(\tau)d\tau \tag{11}$$

where $c > 0$, satisfying the Hurwitz polynomial.

Differentiating both sides of (11) with respect to time t yields

$$\dot{S}(t) = \dot{e}(t) + ce(t). \tag{12}$$

Substituting (10) into (12) yields

$$\dot{S}(t) = ce(t) + \dot{\omega}_{\mathrm{ref}}(t) - (f(x,t) + bu(t) - r(t) - B(x,t)). \tag{13}$$

Equation (13) can be interpreted as the sliding surface dynamics. The condition $S(t) = 0$ defines the system motion that stays on the sliding surface. The objective of this work is to design a robust ILC scheme to steer the sliding surface to become zero within a finite time interval.

A robust ILC controller via sliding mode concept at kth iteration is designed as follows:

$$u_k(t) = b^{-1}\left(ce_k(t) + \dot{\omega}_{\mathrm{ref}}(t) + B(x,t) - \hat{f}(x_k,t) - v_k(t)\right) \tag{14}$$

where k indicates the number of iterations and $x_k(t)$ is the system state variable at kth iteration. Furthermore, $\hat{f}(x_k,t)$ is the recursive control part that is used to learn the unknown state-dependent function $f(x_k,t)$, and it is generated by the following update law:

$$\hat{f}_k(t) = \hat{f}_{k-1}(t) - q\left(\beta_1 \mathrm{sgn}(S_k) + \beta_2 S_k(t)\right) \tag{15}$$

where q, β_1, and β_2 are positive constants and $S_k(t)$ is the sliding surface dynamics at kth iteration.

The SMC law $v_k(t)$ is defined as follows:

$$v_k(t) = -g \cdot \mathrm{sgn}(S_k) - \eta S_k(t) \tag{16}$$

where g is the switching gain and $g > 0$; and η is a positive constant. $\mathrm{sgn}(S)$ is the switching function, which is defined as

$$\mathrm{sgn}(S) = \begin{cases} 1 & \text{if } (S > 0) \\ 0 & \text{if } (S = 0) \\ -1 & \text{if } (S < 0) \end{cases}. \tag{17}$$

Therefore, the sliding surface dynamics (13) can be simplified by inserting the robust ILC law (14)

$$\dot{S}_k(t) = (\hat{f}(x_k,t) - f(x_k,t)) + (v_k(t) + r_k(t)). \tag{18}$$

The above-mentioned equation reveals that if $\hat{f}(x,t)$ can accurately learn from $f(x,t)$ and $v(t)$ can dynamically attenuate the effect of the lumped disturbance $r(t)$, then the sliding surface $S(t)$ will converge to zero.

In SMC, according to the Lyapunov theorem, the minimum switching gain must satisfy $g_{\min} > l_d$ to meet the condition of sliding mode existence and accessibility and resist the system disturbance effectively. However, in practical application, the exact value of the lumped disturbances is difficult to obtain. In addition, large switching gain will lead to the chattering phenomenon, which can excite high-frequency dynamics. To overcome the above-mentioned drawback, an adaptive technique is employed to estimate $r(t)$ online, and the estimated value is used as the compensation part in the control law

$$u_k(t) = b^{-1}\left(ce_k(t) + \dot{\omega}_{\mathrm{ref}}(t) + B(x,t) - \hat{f}(x_k,t) - v_k(t) + \hat{r}_k(t)\right) \tag{19}$$

where $\hat{r}_k(t)$ is the estimated lumped disturbance and is adapted according to the following update law:

$$\dot{\hat{r}}_k(t) = \gamma S_k(t) \tag{20}$$

where γ is the learning constant of the adaptation law and $\gamma > 0$. The estimated error is defined as $\tilde{r}_k(t) = \hat{r}_k(t) - r_k(t)$.

Controller (19), together with (15), (16), and (20), defines the robust ILC controller via adaptive SMC technique.

Substituting (19) into (13) yields

$$\dot{S}_k(t) = (\hat{f}(x_k,t) - f(x_k,t)) + v_k(t) - (\hat{r}_k(t) - r_k(t)). \tag{21}$$

Equation (21) implies that if $\hat{f}(x,t)$ can accurately learn from $f(x,t)$ and $v(t)$ can dynamically eliminate the estimated error $\tilde{r}(t)$, then the sliding surface $S(t)$ will converge to zero.

C. Stability Analysis of the System With the Robust ILC Method

The following theorem constitutes the convergence of the sliding surface dynamics and the output speed tracking error when the robust ILC scheme is applied to the PMSM servo system.

Theorem 1: For system (10), under Assumptions 1–3, the control law proposed in (19) can guarantee that the system output speed tracking errors will asymptotically converge to zero over $[0,\ T]$ when the iteration number approaches infinity.

Proof: To evaluate the convergence property of the output speed tracking error $e(t)$ and the sliding surface dynamics $S(t)$,

the following Lyapunov function is defined at kth iteration:

$$V_k(t) = V_k^1(t) + V_k^2(t) + V_k^3(t) + V_k^4(t) \tag{22}$$

where $V_k^1(t) = \frac{1}{2}\beta_2 S_k^2(t)$, $V_k^2(t) = \beta_1|S_k(t)|$, $V_k^3(t) = \frac{1}{2q}\int_0^t \phi_k^T(\tau)\phi_k(\tau)d\tau$, $\phi_k(t) = \hat{f}_k(t) - f_k(t)$, and $V_k^4(t) = \frac{1}{2\gamma}\beta_2\tilde{r}_k(t)$.

The proof consists of two steps. The first step consists of deriving the difference in the Lyapunov function $V_k(t)$ between two consecutive iterations. Meanwhile, the second step consists of evaluating the convergence of the output tracking error.

1) Differences in the Lyapunov Function Between Two Consecutive Iterations: The difference in the first Lyapunov function $V_k^1(t)$ between kth and $(k-1)$th iterations has the following form:

$$\begin{aligned}\Delta V_k^1(t) = {} & \beta_2\int_0^t S_k(\tau)\phi_k(\tau)d\tau - \beta_2\int_0^t g\,|S_k(\tau)|d\tau \\ & - \eta\beta_2\int_0^t S_k^2(\tau)d\tau - \beta_2\int_0^t S_k(\tau)\tilde{r}(\tau)d\tau \\ & - \frac{1}{2}\beta_2 S_{k-1}^2(t).\end{aligned} \tag{23}$$

See Appendix A for more details on the derivation of $\Delta V_k^1(t)$.

The difference in the second Lyapunov function $V_k^2(t)$ between kth and $(k-1)$th iterations is shown as follows:

$$\begin{aligned}\Delta V_k^2(t) = {} & \beta_1\int_0^t \mathrm{sgn}(S_k)\phi_k(\tau)d\tau - \beta_1\int_0^t \eta\,|S_k(\tau)|\,d\tau \\ & + \beta_1\int_0^t \mathrm{sgn}(S_k)\left(-g\cdot\mathrm{sgn}(S_k) - \tilde{r}(\tau)\right)d\tau \\ & - \beta_1\,|S_{k-1}(t)|\,.\end{aligned} \tag{24}$$

See Appendix B for more details on the derivation of $\Delta V_k^2(t)$.

The difference in the third Lyapunov function $V_k^3(t)$ between kth and $(k-1)$th iterations can be expressed as

$$\begin{aligned}\Delta V_k^3(t) = {} & -\frac{q}{2}\int_0^t \left(\beta_1\mathrm{sgn}(S_k) + \beta_2 S_k(\tau)\right)^2 d\tau \\ & - \beta_1\int_0^t \mathrm{sgn}(S_k)\phi_k(\tau)d\tau \\ & - \beta_2\int_0^t S_k(\tau)\phi_k(\tau)d\tau.\end{aligned} \tag{25}$$

See Appendix C for more details on the derivation of $\Delta V_k^3(t)$.

The difference in the fourth Lyapunov function $V_k^4(t)$ between kth and $(k-1)$th iterations has the following form:

$$\Delta V_k^4(t) = \beta_2\int_0^t S_k(\tau)\tilde{r}_k(\tau)d\tau - \frac{1}{2\gamma}\beta_2\tilde{r}_{k-1}^2(t). \tag{26}$$

See Appendix D for more details on the derivation of $\Delta V_k^4(t)$.

2) Convergence of the Output Tracking Error: Based on the differences in $V_k^1(t)$, $V_k^2(t)$, $V_k^3(t)$, and $V_k^4(t)$ between two consecutive iterations, we go further to prove the convergence of both the sliding surface dynamics and the output speed tracking error.

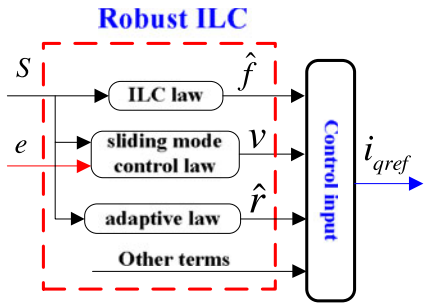

Fig. 2. Block diagram of the robust ILC controller.

The difference in the Lyapunov function $V_k(t)$ between kth and $(k-1)$th iteration can be obtained by adding all of them

$$\begin{aligned}\Delta V_k(t) &= \Delta V_k^1(t) + \Delta V_k^2(t) + \Delta V_k^3(t) + \Delta V_k^4(t) \\ &= -\beta_2\int_0^t g\,|S_k(\tau)|d\tau - \eta\beta_2\int_0^t S_k^2(\tau)d\tau \\ &\quad - \frac{1}{2}\beta_2 S_{k-1}^2(t) \\ &\quad - \beta_1\,|S_{k-1}(t)| + \beta_1\int_0^t \mathrm{sgn}(S_k)\left(-g\mathrm{sgn}(S_k)\right. \\ &\quad \left.-\tilde{r}(\tau)\right)d\tau \\ &\quad - \frac{q}{2}\int_0^t \left(\beta_1\mathrm{sgn}(S_k) + \beta_2 S_k(\tau)\right)^2 d\tau \\ &\quad - \beta_1\eta\int_0^t |S_k(\tau)|\,d\tau \\ &\quad - \frac{1}{2\gamma}\beta_2\tilde{r}_{k-1}^2(t) \\ &\le \beta_1\int_0^t \mathrm{sgn}(S_k)\left(-g\cdot\mathrm{sgn}(S_k) - \tilde{r}(\tau)\right)d\tau.\end{aligned} \tag{27}$$

Let switching gain g satisfy $g \ge |\tilde{r}|$, and then the above-mentioned inequality can be further simplified as

$$\Delta V_k(t) \le 0 \tag{28}$$

which is negative definite when $S_k(t) \ne 0, t \in [0, T]$. This result concludes that the Lyapunov function $V_k(t)$ is convergent. In addition, positive definiteness $V_k(t)$ can ensure the convergence of the sliding surface dynamics $S_k(t)$ to zero. Since the sliding surface dynamics (11) is selected to be Hurwitz, the output speed tracking error $e(t)$ is convergent asymptotically. Thus, the proof of Theorem 1 is completed.

From (27) and (28), it can be seen that the minimum switching gain simply needs to satisfy $g_{\min} \ge |\tilde{r}|$ to guarantee the system stability and robustness. It means that the adaptive technique can reduce the minimum switching gain and thus alleviate sliding mode chattering on the premise of the assurance of system robustness.

A block diagram is employed, as shown in Fig. 2, to depict the configuration of the proposed robust ILC controller.

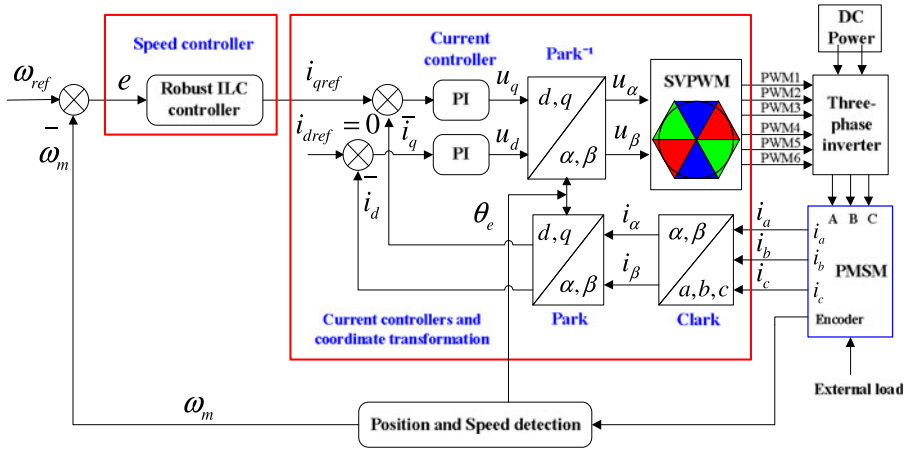

Fig. 3. Structure diagram of the PMSM servo system based on robust ILC scheme.

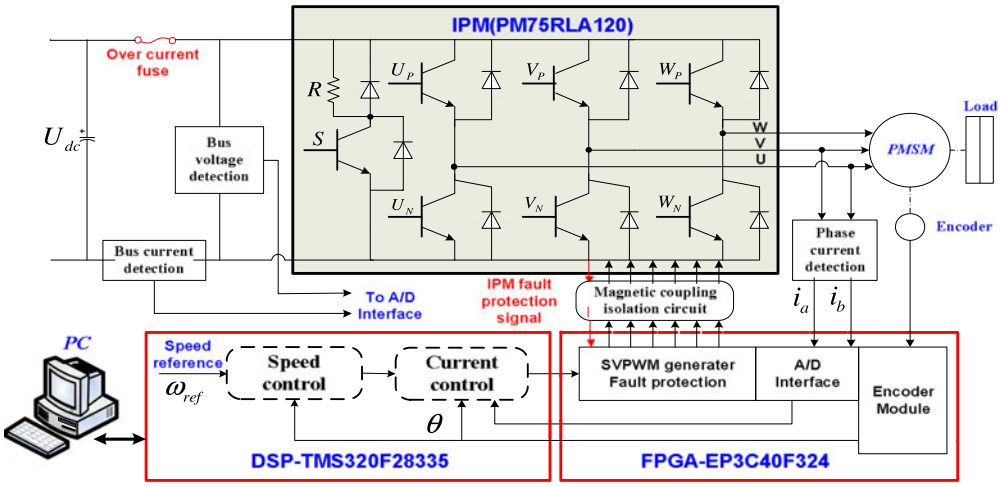

Fig. 4. Configuration of the DSP and FPGA-based experimental setup.

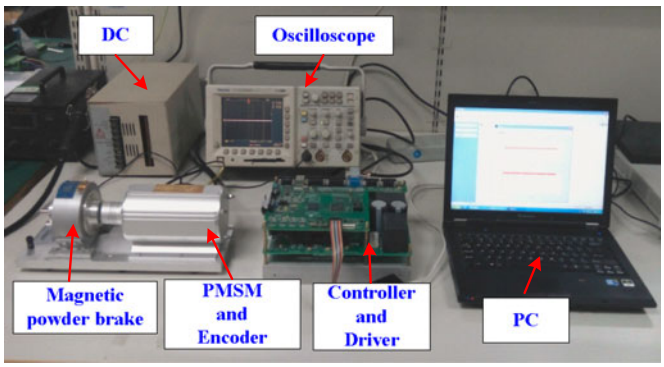

Fig. 5. Photograph of the experimental platform.

TABLE I
PMSM PARAMETERS

Description	Value
Rated power	200 W
Rated speed	3000 r/min
Armature resistance	15.42 Ω
Armature inductance	30.08 mH
Torque constant	0.41 Nm/A
Number of pole pairs	4
Inertia	0.138 kg·cm²

V. IMPLEMENTATION OF DRIVE SYSTEM

Fig. 3 shows the overall structure diagram of the PMSM servo system based on the robust ILC scheme for torque ripple minimization. The FOC method is utilized to control the PMSM. The robust ILC controller is employed as the speed controller to generate the q-axis reference current i_{qref}. PI current controllers are adopted in the inner loop to generate the control voltages.

The configuration of the experimental setup is shown in Fig. 4, whereas Fig. 5 shows the photograph of the experimental platform. The parameters of the surface-mounted PMSM (delta-connected stator windings) used are listed in Table I. An incremental optical encoder is employed for measurement of the digital position and the resolution ratio is 2500 pulse per revolution (ppr). A quadruplicated frequency is achieved using

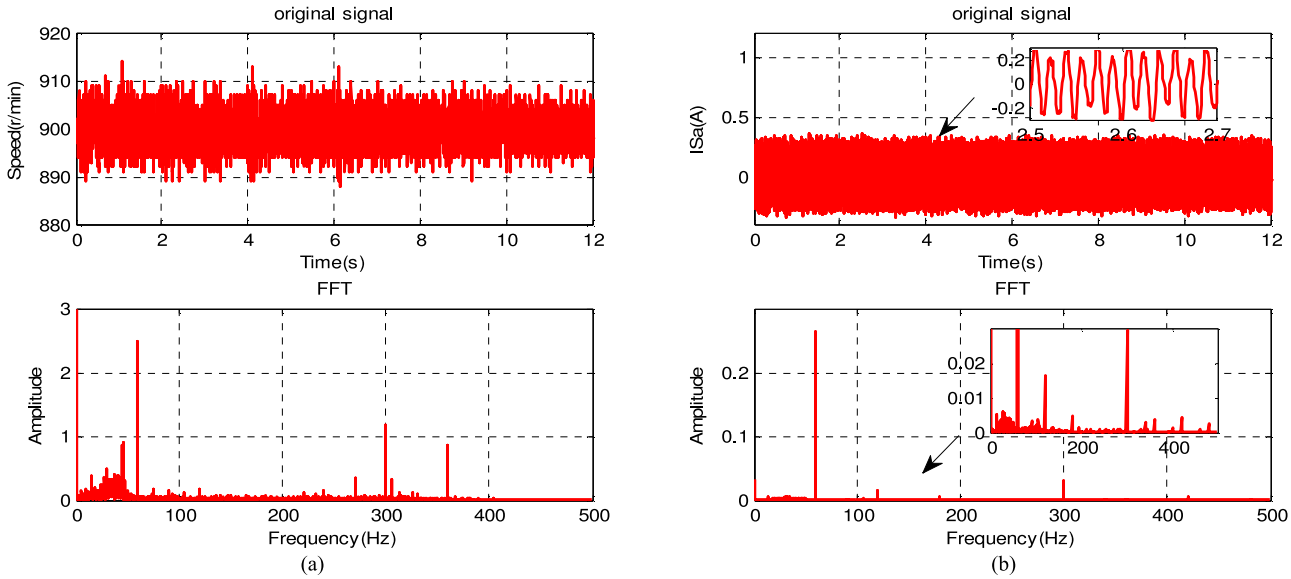

Fig. 6. Experimental results of the PI control at 900 r/min: (a) speed response; (b) phase current I_a response.

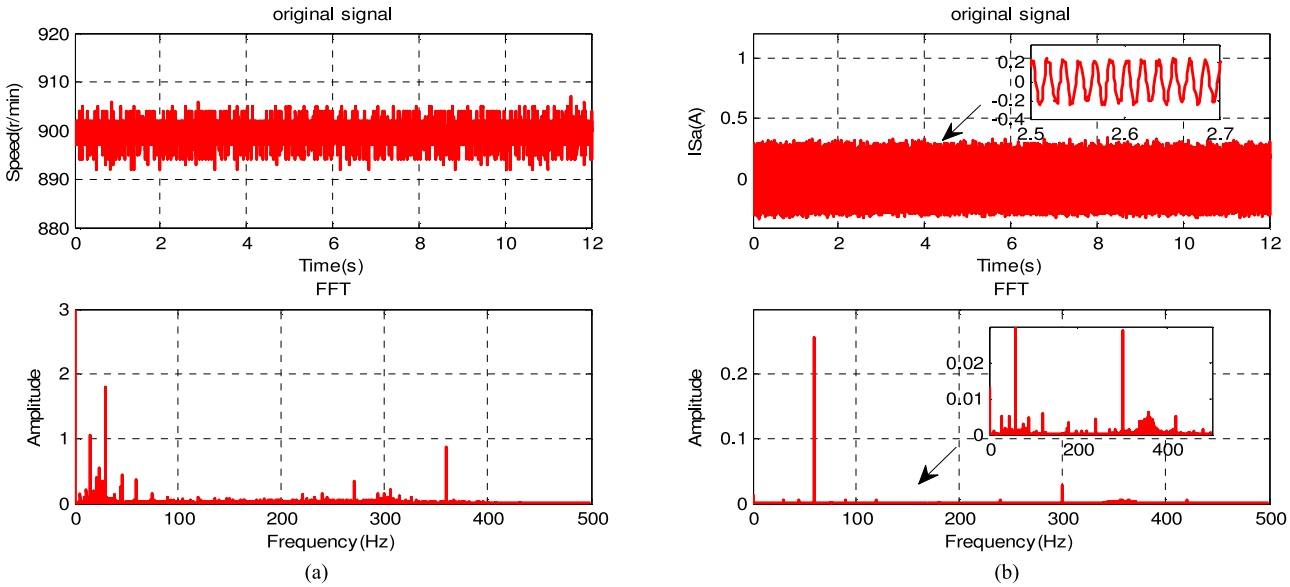

Fig. 7. Experimental results of the PI-ILC control at 900 r/min : (a) speed response; (b) phase current I_a response.

a field programmable gate array (FPGA), and in practice, the resolution ratio can be 10 000 ppr. Speed detection is realized using the FPGA. The proposed overall control scheme is realized in DSP-TMS320F28335 and FPGA-EP3C40F324-based drive setup. The proposed robust ILC algorithm is implemented using a C-program in digital signal processor (DSP).

The performance evaluation of the proposed robust ILC scheme is presented in the following section.

VI. Experimental Results and Discussions

In this section, to verify the effectiveness of the proposed robust ILC scheme, experiments are carried out using the DSP-FPGA-based PMSM drive system described in the previous section.

Experiments are conducted to evaluate the effectiveness of the proposed robust ILC scheme under various operating conditions, including low speed, high speed, light load, heavy load, sudden load, and sudden unload conditions. The traditional PI method is applied to define the original torque ripple situation of the PMSM control system without compensation. The PI-ILC scheme for comparison is shown in Fig. 1, and the ILC law is chosen to be P type, which is simple and widely used and can be expressed as follows:

$$u_{k+1}(t) = u_k(t) + \xi e_{k+1}(t). \tag{29}$$

The parameters of the current PI controllers in the three methods are all the same: q-axis controller: $K_{ip} = 5.0$ and $K_{ii} = 0.5$; d-axis controller: $K_{ip} = 5.0$ and $K_{ii} = 0.5$. The

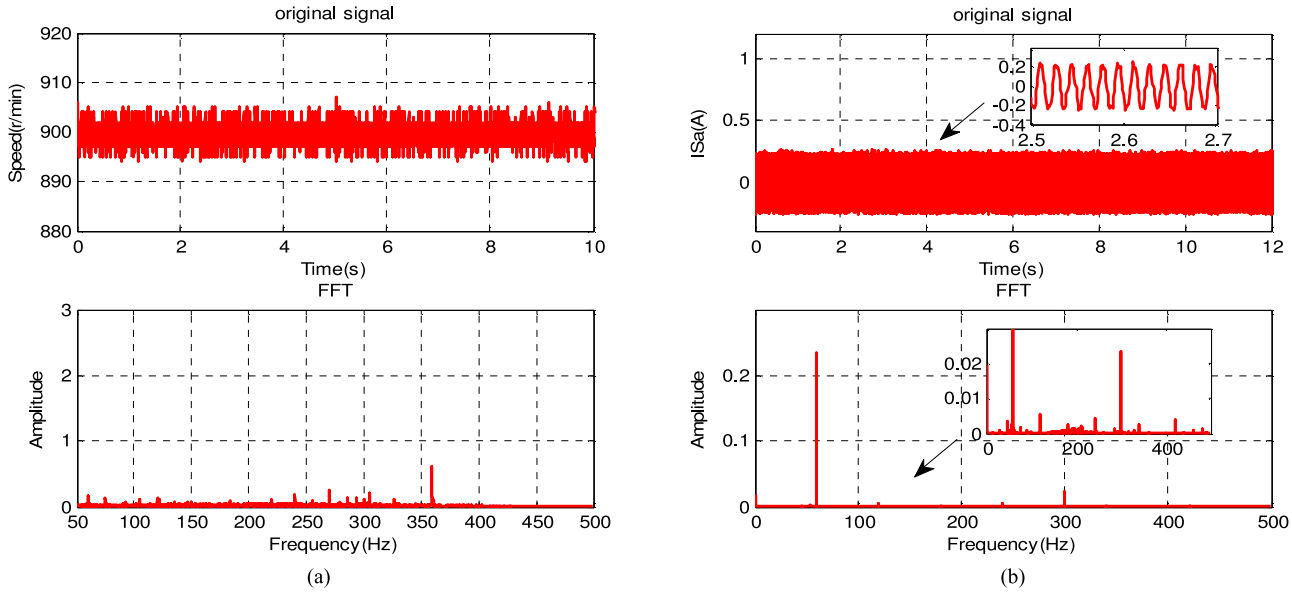

Fig. 8. Experimental results of the robust ILC control at 900 r/min: (a) speed response; (b) phase current I_a response.

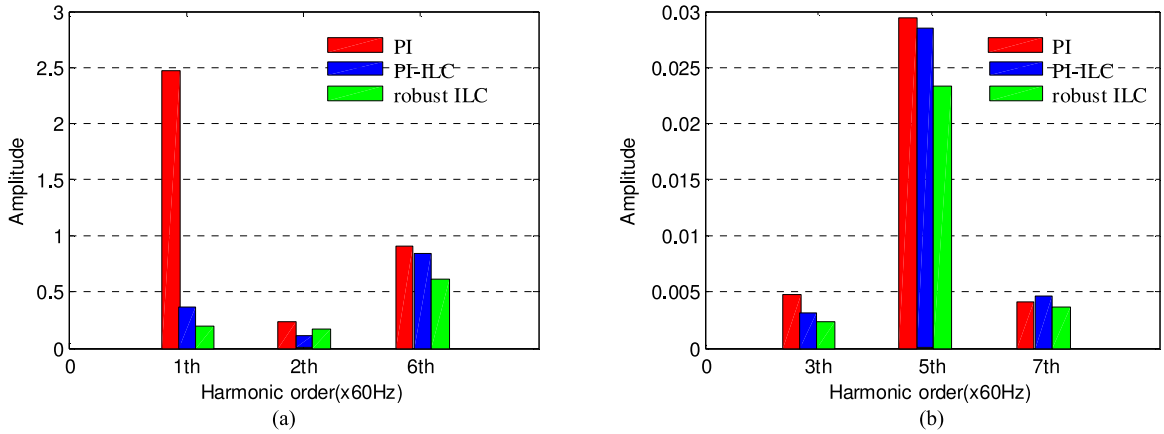

Fig. 9. Comparison results of the harmonic amplitudes with the PI, PI-ILC, and robust ILC methods: (a) comparison results of the harmonic amplitudes in speed; (b) comparison results of the harmonic amplitudes in phase current I_a.

TABLE II
DETAILS OF THE HARMONICS IN SPEED

Control method	Amplitude of harmonics in speed		
	1st	2nd	6th
PI	2.49	0.20	0.89
PI-ILC	0.35	0.10	0.83
Robust ILC	0.18	0.13	0.60

TABLE III
DETAILS OF THE HARMONICS IN CURRENT

Control method	Amplitude of harmonics in I_a		
	3rd	5th	7th
PI	0.0049	0.0295	0.0045
PI-ILC	0.0032	0.0286	0.0049
Robust ILC	0.0025	0.0235	0.0040

parameters of the PI-ILC speed controller are $K_{sp} = 0.015$, $K_{si} = 0.0003$, and $\xi = 0.004$. The parameters of the robust ILC speed controller are $c = 5$, $k = 500$, $\eta = 180$, $q = 0.1$, $\beta_1 = 0.4$, $\beta_2 = 0.3$, and $\gamma = 0.003$. The sampling frequency for the speed and current controllers is 1 and 15 kHz, respectively. Notably, the iterative cycle of the ILC controller is different from the system control cycle. To reject the periodic ripples, the iterative cycle should be the same as the period of the ripples. Therefore, the iterative cycle T_{iter} should be chosen as $T_{\text{iter}} = 2\pi/p\omega_m$.

A. *Effectiveness of Robust ILC in Torque Ripple Minimization Under Different Operating Speed Conditions*

In order to demonstrate the ability of the robust ILC to minimize torque ripples under different operating speed conditions,

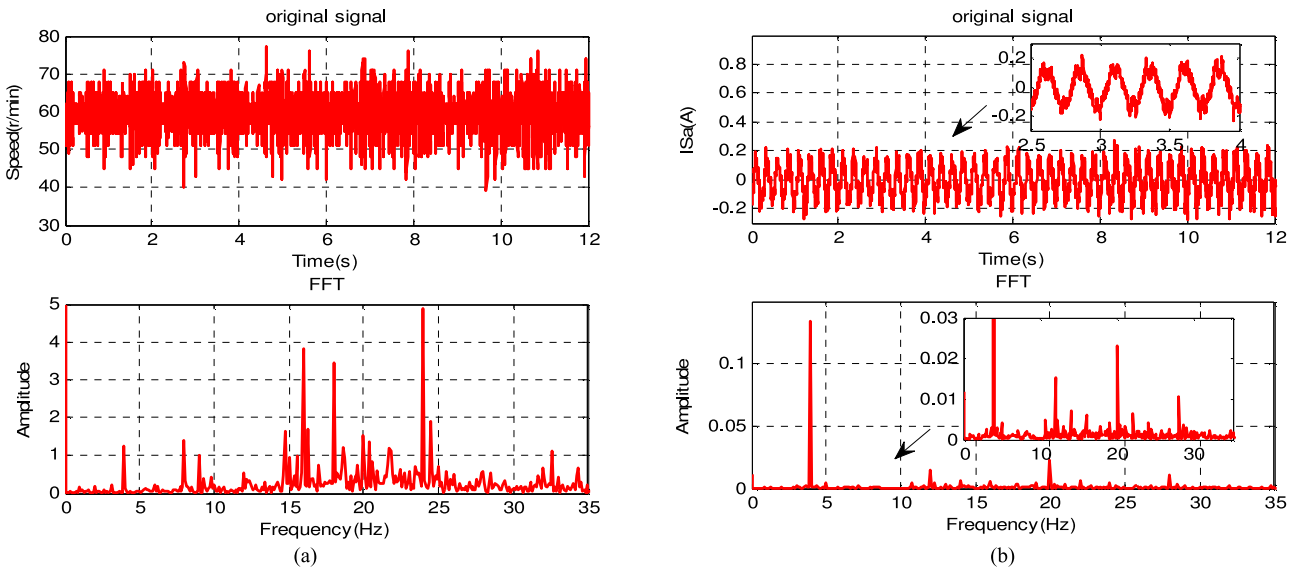

Fig. 10. Experimental results of the PI control at 60 r/min: (a) speed response; (b) phase current I_a response.

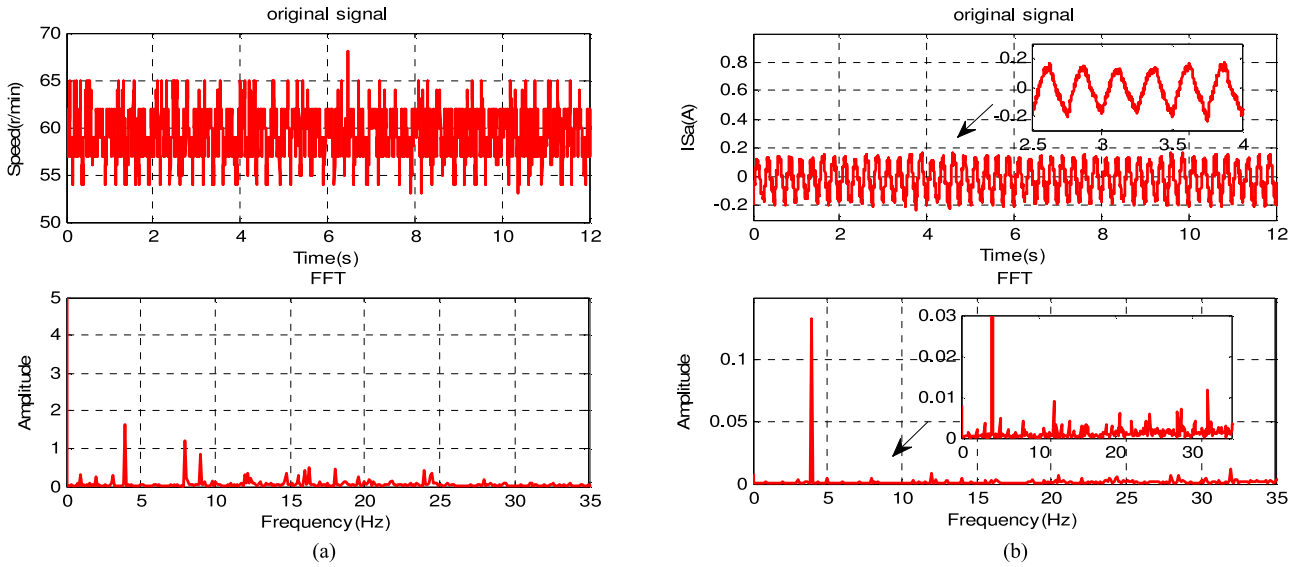

Fig. 11. Experimental results of the PI-ILC control at 60 r/min: (a) speed response; (b) phase current I_a response.

experiments are carried out in both high speed (900 r/min) and low speed (60 r/min) conditions, with the PI, PI-ILC, and robust ILC methods.

To be precise, only the 1st, 2nd, and 6th speed ripple harmonics and only the 3rd, 5th, and 7th phase current ripple harmonics are picked up, since they are pertinent to the assessment of the effectiveness of the proposed robust ILC method in torque ripple minimization.

The experimental results of the PI, PI-ILC, and robust ILC methods at 900 r/min are shown in Figs. 6–9. Figs. 6(a), 7(a), and 8(a) show the speed response and Fourier analysis of the corresponding speed.Figs. 6(b), 7(b), and 8(b) show the phase current I_a response and the Fourier analysis of the corresponding current. The detailed experimental results of the harmonics in speed ripples and phase current ripples are shown in Tables II and III. Furthermore, the harmonic amplitude results of the three different methods are compared in Fig. 9 in the shape of a histogram.

The experimental results demonstrate that, at the speed of 900 r/min, the robust ILC method achieves a satisfactory torque ripple minimization performance, as the speed and phase-current I_a responses show the smallest ripple harmonic amplitude under robust ILC control compared to the PI and PI-ILC methods. Consider the sixth harmonics in speed for instance. In the PI control, the sixth harmonics amplitude is 0.89, whereas in the PI-ILC and robust ILC, the amplitudes are reduced to 0.83 and 0.6, respectively. Similarly, consider the fifth harmonics in phase-current I_a for instance. In the PI control, the fifth

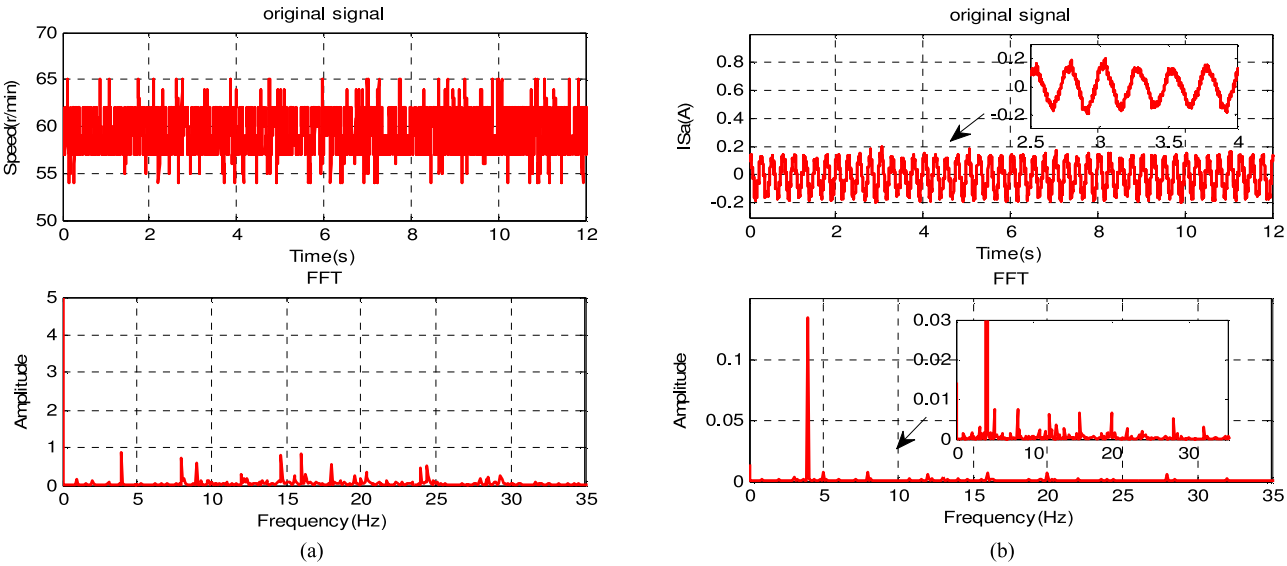

Fig. 12. Experimental results of the robust ILC control at 60 r/min: (a) speed response; (b) phase current I_a response.

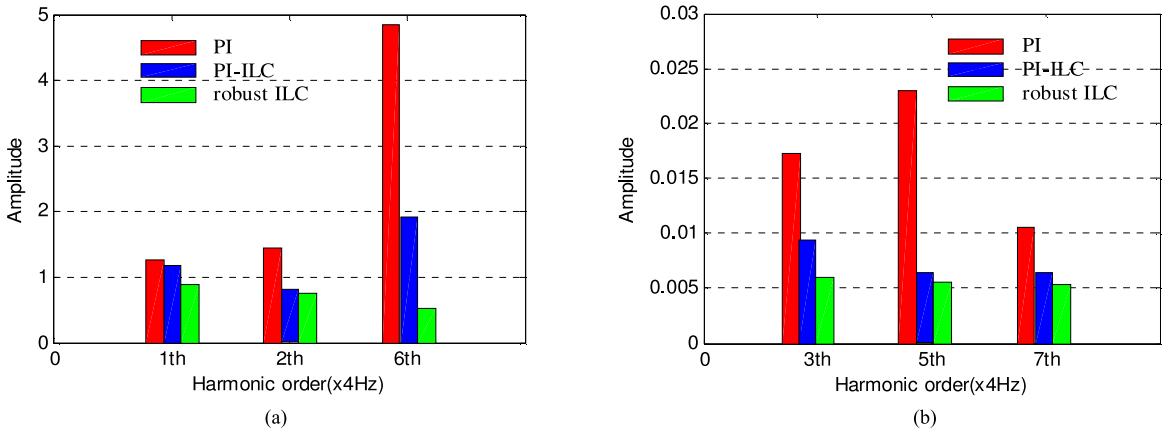

Fig. 13. Comparison results of the harmonic amplitudes with the PI, PI-ILC, and robust ILC methods: (a) comparison results of the harmonic amplitudes in speed; (b) comparison results of the harmonic amplitudes in phase current I_a.

TABLE IV
DETAILS OF THE HARMONICS IN SPEED

Control method	Amplitude of harmonics in speed		
	1st	2nd	6th
PI	1.25	1.38	4.87
PI-ILC	1.14	0.725	1.92
Robust ILC	0.87	0.72	0.46

TABLE V
DETAILS OF THE HARMONICS IN CURRENT

Control method	Amplitude of harmonics in I_a		
	3rd	5th	7th
PI	0.0154	0.0231	0.0106
PI-ILC	0.0090	0.0066	0.0064
Robust ILC	0.0061	0.0055	0.0053

harmonics amplitude is 0.0295, whereas in the PI-ILC and robust ILC, the amplitudes are reduced to 0.0286 and 0.0235, respectively. The speed steady-state error is maintained at ± 5 r/min, within one encoder pulse when the robust ILC method is employed. At a high operating speed, these torque pulsations are naturally filtered off by the rotor or load inertias to some extent, and thus, the ripples in speed and phase-current are fewer than those at the low operating speed.

The experimental results of the PI, PI-ILC, and robust ILC methods at 60 r/min are shown in Figs. 10–13. Figs. 10(a), 11(a), and 12(a) show the speed response and the corresponding speed spectrum analysis.Figs. 10(b), 11(b), and 12(b) show the phase current I_a response and the corresponding current spectrum analysis.The detailed experimental results of the harmonics in speed and phase current ripples are listed in Tables IV and V. The harmonic amplitude results of the three different methods

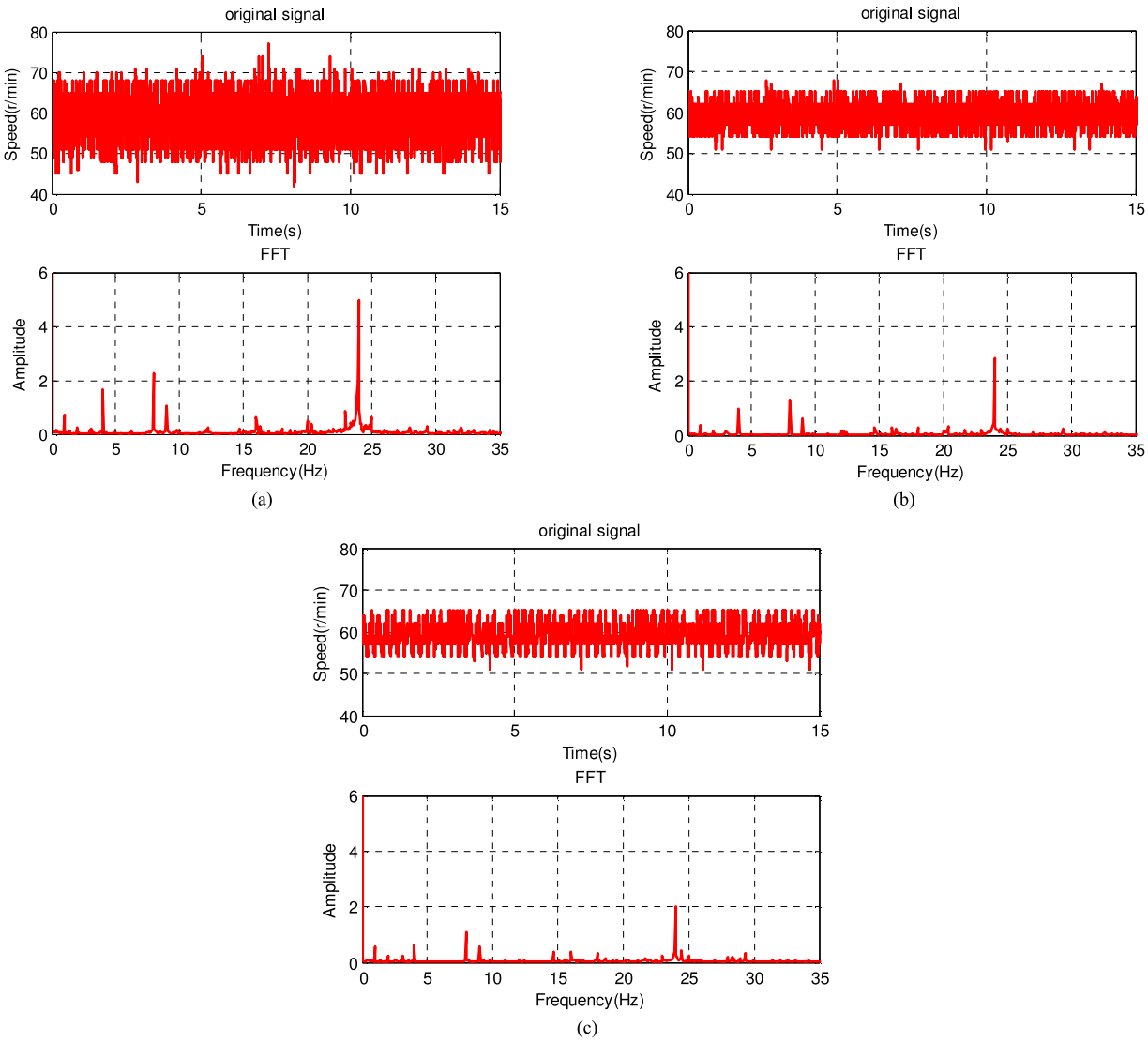

Fig. 14. Experimental results under 30% load condition: (a) speed response of the PI method; (b) speed response of the PI-ILC method; (c) speed response of the robust ILC method.

are compared in Fig. 13 in the shape of a histogram, for the sake of clarity.

From the experimental results presented, it is evident that at low speed, the torque ripples reflected back in the motor speed are more serious than at high speed, and both the PI-ILC and robust ILC methods are able to reduce the speed ripple harmonics as well as the current ripple harmonics to a certain extent. Consider the sixth harmonics in speed ripples for instance. In the PI control, the sixth harmonics amplitude is 4.87, whereas in the PI-ILC control, the amplitude is reduced to 1.92. In the robust ILC control, the amplitude is further reduced to 0.46. Similarly, consider the fifth harmonics in I_a for instance. In the PI control, the fifth harmonics amplitude is 0.0231, whereas in the PI-ILC control, the amplitude is reduced to 0.0066. In the robust ILC control, the amplitude is further reduced to 0.0055. The speed steady-state error is controlled to be within ± 5 r/min with the robust ILC method. Obviously, it can be concluded that the robust ILC guarantees better performance in the minimization of torque ripples compared to the PI-ILC method.

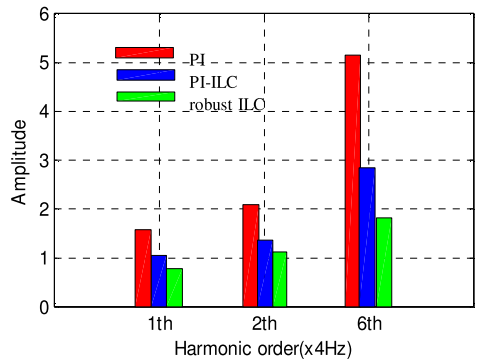

Fig. 15. Comparison results of the harmonic amplitudes in speed.

According to the above-mentioned experimental results, the effectiveness of the proposed robust ILC scheme in suppressing torque ripples has been verified under various operating speeds.

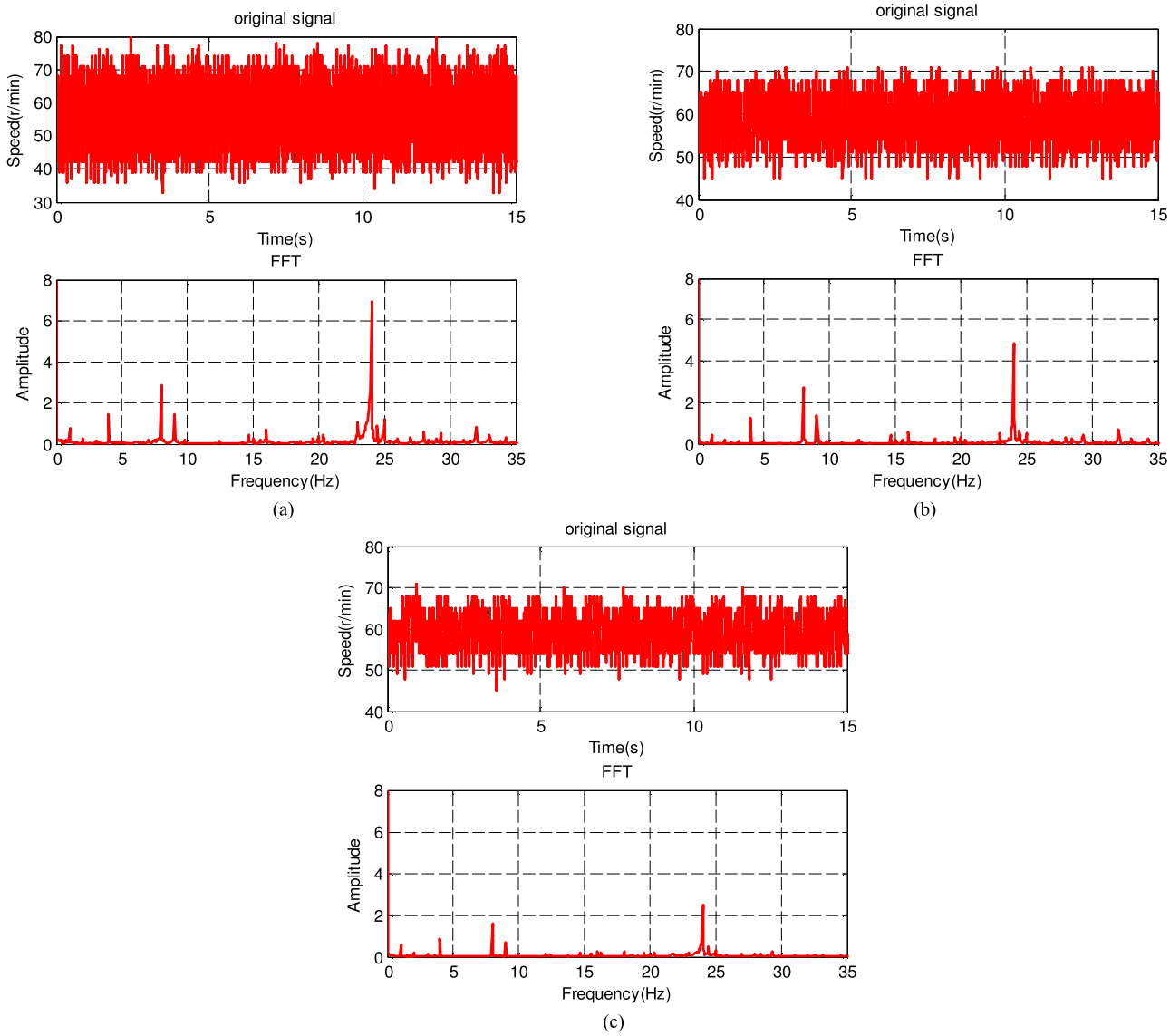

Fig. 16. Experimental results under 78% load condition: (a) speed response of the PI method; (b) speed response of the PI-ILC method; (c) speed response of the robust ILC method.

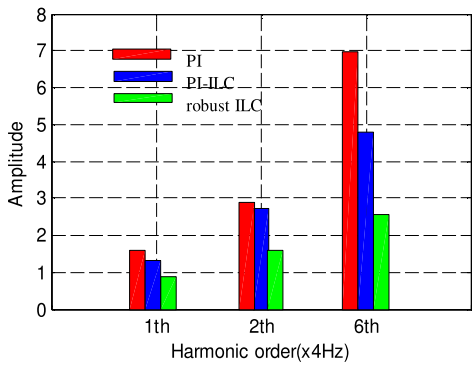

Fig. 17. Comparison results of the harmonic amplitudes in speed.

B. Effectiveness of Robust ILC in Torque Ripple Minimization Under Different Load Conditions

In order to investigate the effectiveness of the robust ILC in torque ripple minimization under different load conditions, experiments are carried out in both 30% (light load) and 78% (heavy load) load conditions, with the PI, PI-ILC, and robust ILC methods. Since the influence of torque ripples in high-speed operating condition is relatively small, experiments are only carried out in the low-speed operating condition (60 r/min). The speed response results are presented to illustrate the effectiveness of the robust ILC, which are sufficient. The experimental results are shown in Figs. 14–17.

Fig. 14 shows the speed response and the corresponding speed spectrum analysis with different control methods, under the conditions of a speed reference of 60 r/min and 30% load. The detailed experimental results of the harmonics in speed ripples are listed in Table VI. Furthermore, the comparisons of the harmonic amplitude results of the three different methods are shown in Fig. 15 in the shape of a histogram. We can see that speed ripple harmonics are reduced by PI-ILC to a certain extent. Further reduction is possible using the robust ILC method. Consider the sixth harmonics in speed ripples for instance. In

TABLE VI
DETAILS OF THE HARMONICS IN SPEED

Control method	Amplitude of harmonics in speed		
	1st	2nd	6th
PI	1.48	2.1	5.15
PI-ILC	1.02	1.31	2.85
Robust ILC	0.72	1.10	1.95

TABLE VII
DETAILS OF THE HARMONICS IN SPEED

Control method	Amplitude of harmonics in speed		
	1st	2nd	6th
PI	1.52	2.89	6.98
PI-ILC	1.27	2.60	4.85
Robust ILC	0.93	1.62	2.49

the PI control, the sixth harmonics amplitude is 5.15, whereas in the PI-ILC control the amplitude is reduced to 2.85. In the robust ILC control, the amplitude is further reduced to 1.95. The experimental results demonstrate that, under the light-load condition, the robust ILC method achieves a satisfactory torque minimization performance compared to the PI-ILC method.

Fig. 16 shows the speed response and the corresponding speed spectrum analysis with different control methods, under the conditions of a speed reference of 60 r/min and 78% load. The detailed experimental results of the harmonics in speed ripples are listed in Table VII. From the presented experimental results, it can be found that the PI-ILC can suppress the torque ripple harmonics effectively. The torque ripple harmonics is further decreased, when the robust ILC is employed. Consider the sixth harmonics in speed ripples for instance. In the PI control, the sixth harmonics amplitude is 6.98. In the PI-ILC control, the sixth harmonics amplitude is reduced to 4.85. In the robust ILC control, the amplitude is reduced to 2.49. The comparisons of the harmonic amplitude results of the three different methods are shown in Fig. 17 in the shape of a histogram. The experimental results demonstrate that, under the heavy-load condition, the robust ILC method also guarantees better performance in torque ripple minimization, compared to the PI-ILC method.

According to the above-mentioned results, the effectiveness of the proposed robust ILC scheme is verified in torque ripple minimization under various load conditions.

C. Verification of Robust ILC Antidisturbance Ability

In order to test the antidisturbance ability (i.e., the ability to suppress nonperiodic speed ripples) of the robust ILC scheme, experiments were carried out under the impact of sudden load and sudden unload disturbances. The load torque $T_L = 0.6$ Nm was added suddenly and removed after a duration of $t = 8$ s in all the experiments presented in this section. The load torque of 0.6 Nm acted as the disturbance on the load side. The sudden load and unload were realized by the magnetic powder brake. The reference high and low speeds are set to be 900 and 60 r/min, respectively.

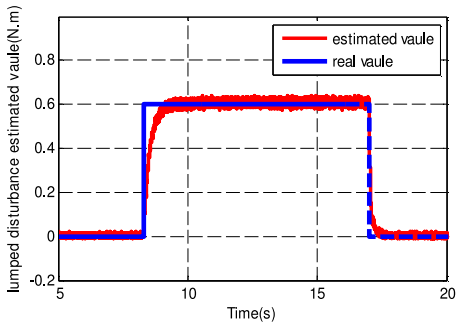

Fig. 18. Estimated results of the adaptive algorithm.

TABLE VIII
COMPARISONS OF ANTIDISTURBANCE PERFORMANCE INDICES AT HIGH SPEED

Control Scheme	PI-ILC	Robust ILC
Maximum speed fluctuation (r/min)	38	20
Speed adjustment time (s)	0.7	0.38
Overshoot in I_q (A)	0.65	0.18
I_q adjustment time (s)	0.65	0.32

TABLE IX
COMPARISONS OF ANTIDISTURBANCE PERFORMANCE INDICES AT LOW SPEED

Control Scheme	PI-ILC	Robust ILC
Maximum speed fluctuation (r/min)	36	21
Speed adjustment time (s)	0.77	0.45
Overshoot in I_q (A)	0.55	0.25
I_q adjustment time (s)	0.72	0.42

Considering the robustness of the PMSM servo system, the comparison of the experimental results of the PI-ILC and robust ILC methods is shown in Figs. 18–20. Fig. 18 shows the estimated results of the adaptive algorithm. Fig. 19 shows the dynamic responses of the speed, phase current I_a, and q axis current I_q when the motor is running at high speed (i.e., 900 r/min) with the PI-ILC and robust ILC control method, respectively. Fig. 20 shows the arrangement in the same sequence, but with the motor running at low speed, i.e., 60 r/min.

From the experimental results, it is evident that the adaptive algorithm can estimate the lumped disturbance exactly and quickly, and the robust ILC method has a satisfactory antidisturbance ability compared to the PI-ILC method. The experimental results show that the robust ILC control gives a smaller fluctuation in speed and I_a, and a smaller overshoot in I_q irrespective of the high or low speed operating conditions. In addition, the speed, I_a, and I_q are guaranteed to be restored to their original values much faster.

For the sake of clarity, the characteristics of the speed and I_q response are chosen to be the antidisturbance performance indices. The details of the antidisturbance performance indices with respect to the PI-ILC and robust ILC method under different operating speeds are shown in Tables VIII and IX. It can be

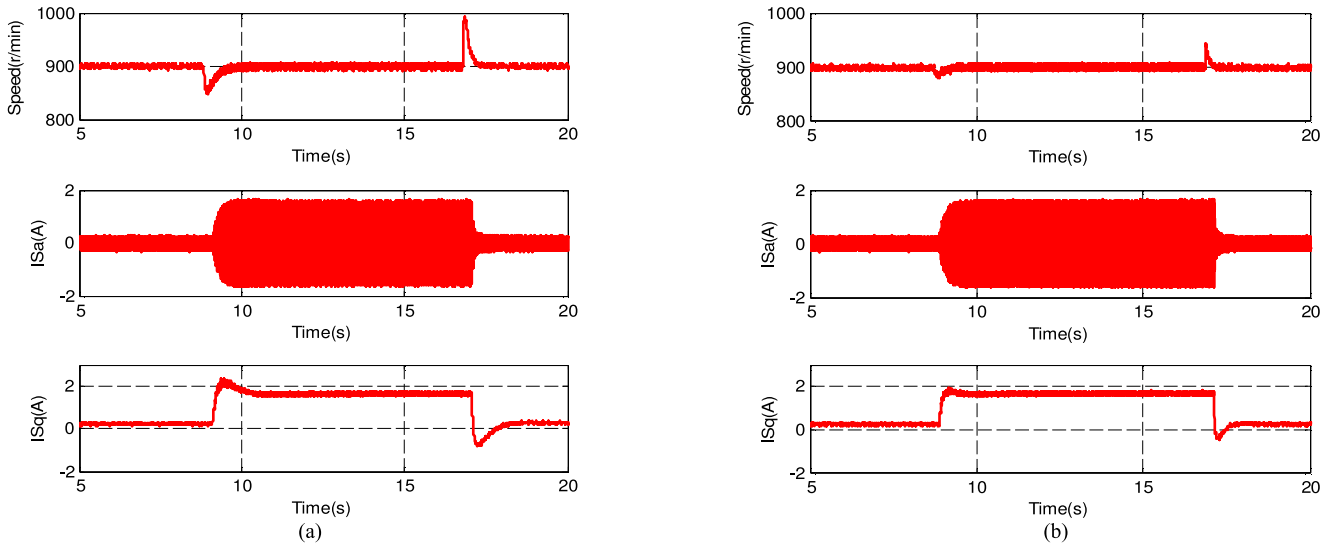

Fig. 19. Experimental results under sudden load disturbance at a speed of 900 r/min with different methods: (a) experimental results of the PI-ILC method; (b) experimental results of the robust ILC method.

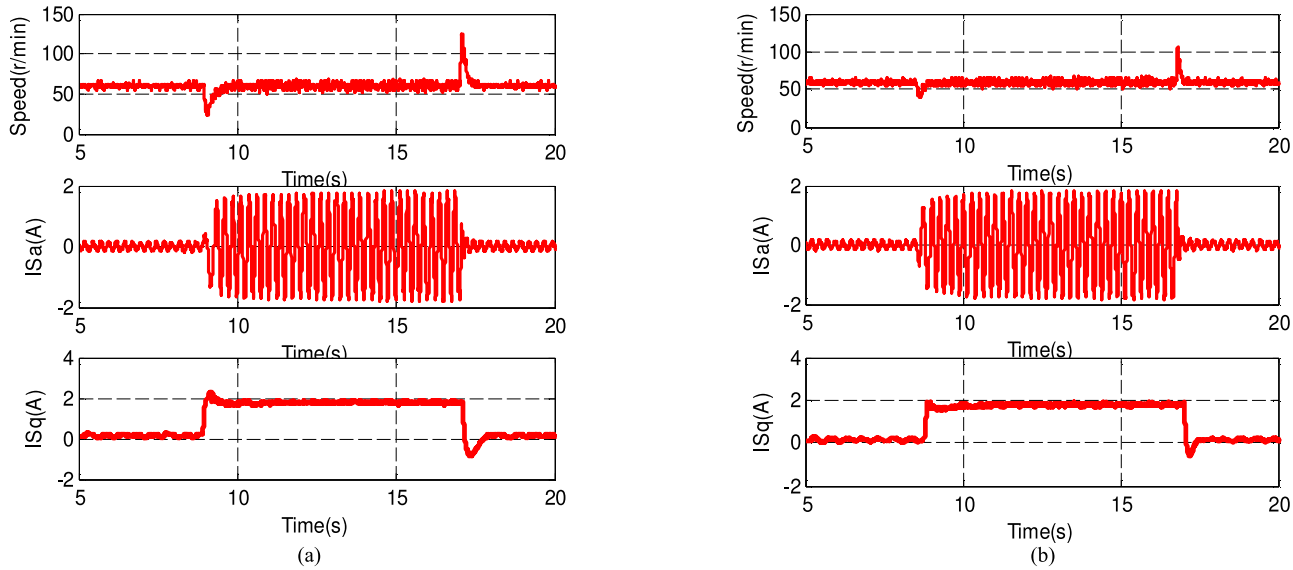

Fig. 20. Experimental results under sudden load disturbance at a speed of 60 r/min with different methods: (a) experimental results of the PI-ILC method; (b) experimental results of the robust ILC method.

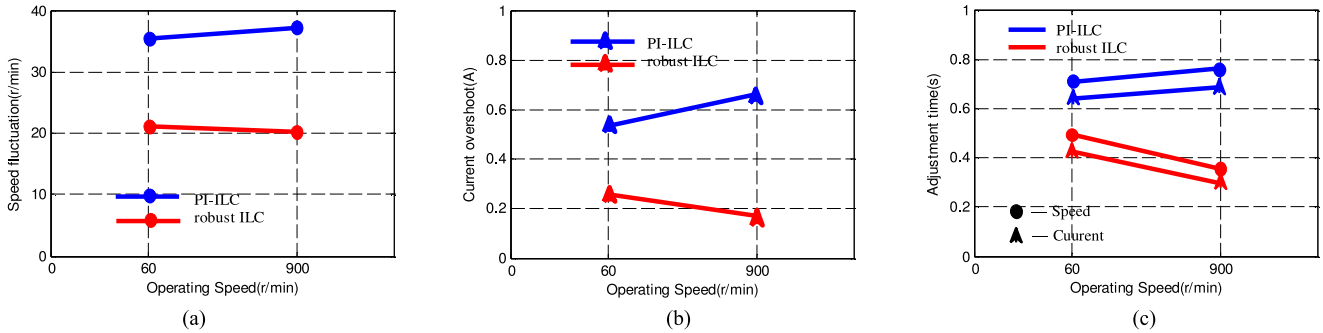

Fig. 21. Comparisons of performance indices under different control methods: (a) comparisons of speed fluctuation; (b) comparisons of current overshoot; (c) comparisons of adjustment time of speed and current.

found that when the motor is operating at the speed of 900 r/min and a sudden load disturbance of 0.6 Nm is added, the maximum speed fluctuation under the PI-ILC control is 38 r/min, whereas the robust ILC method reduces the maximum speed fluctuation to 20 r/min. Furthermore, the maximum speed fluctuation is reduced by 2% compared to the PI-ILC method, and the adjustment time needed for the speed to return to its original value is as small as 0.38 s under the robust ILC control. When the motor is operating at a speed of 60 r/min, the PI-ILC method shows a maximum speed fluctuation of 36 r/min, whereas the robust ILC method gives a smaller fluctuation of 21 r/min. Furthermore, the maximum speed fluctuation is reduced by 25%, and a much smaller adjustment time of 0.45 s is needed for the speed to return to the original value. The overall comparisons of the performance indices are shown in Fig. 21.

It can be concluded that the robust ILC has an overwhelming advantage with respect to disturbance rejection compared to the PI-ILC method.

VII. Conclusion

A robust ILC strategy via adaptive SMC is presented in this paper, for the purpose of torque ripple minimization as well as improvement of the antidisturbance ability of the PMSM speed control system. ILC is a reasonable choice for torque ripple minimization because of the periodic nature of torque ripples and therefore, the speed ripples. The SMC is synthesized into the design of ILC controller, to ensure that the system is more robust to disturbances. Adaptive technique is utilized to estimate the lumped disturbances of the system. The estimated disturbance is utilized to compensate the robust ILC controller, which can reduce the minimum switching gain and thus alleviate the system sliding mode chattering simultaneously. Experimental investigations were conducted on an integrated DSP-FPGA-based PMSM platform. The PMSM servo system was operated at different speed and load conditions to evaluate the proposed robust ILC method. The effectiveness of the proposed robust ILC scheme was demonstrated by the experimental results.

Appendix A

The difference in the first Lyapunov function $V_k^1(t)$ between $k\text{th}$ and $(k-1)\text{th}$ iterations has the following form:

$$\Delta V_k^1(t) = \frac{1}{2}\beta_2 S_k^2(t) - \frac{1}{2}\beta_2 S_{k-1}^2(t). \tag{30}$$

Differentiating $\frac{1}{2}S_k^2(t)$ with respect to time t yields

$$\frac{d}{dt}\left(\frac{1}{2}S_k^2(t)\right) = S_k(t)\dot{S}_k(t). \tag{31}$$

Based on (30) and (31), it follows that:

$$\Delta V_k^1(t) = \beta_2 \int_0^t S_k(\tau)\dot{S}_k(\tau)d\tau - \frac{1}{2}\beta_2 S_{k-1}^2(t). \tag{32}$$

Substituting (21) into the above-mentioned equation and considering (16), we have

$$\begin{aligned}\Delta V_k^1(t) &= \beta_2 \int_0^t S_k(\tau)\left(\hat{f}(x_k,\tau) - f(x_k,\tau)\right. \\ &\quad \left. + v_k(\tau) - (\hat{r}(\tau) - r(\tau))\right)d\tau - \frac{1}{2}\beta_2 S_{k-1}^2(t) \\ &= \beta_2 \int_0^t S_k(\tau)\phi_k(\tau)d\tau - \eta\beta_2 \int_0^t S_k^2(\tau)d\tau \\ &\quad - \beta_2 \int_0^t g\cdot \mathrm{sgn}(S_k)S_k(\tau)d\tau - \beta_2 \int_0^t S_k(\tau)\tilde{r}(\tau)d\tau \\ &\quad - \frac{1}{2}\beta_2 S_{k-1}^2(t). \end{aligned} \tag{33}$$

Considering the fact that $\mathrm{sgn}(S_k)S_k = |S_k|$, the above-mentioned equation can be simplified as

$$\begin{aligned}\Delta V_k^1(t) &= \beta_2 \int_0^t S_k(\tau)\phi_k(\tau)d\tau - \beta_2 \int_0^t g\,|S_k(\tau)|d\tau \\ &\quad - \eta\beta_2 \int_0^t S_k^2(\tau)d\tau - \beta_2 \int_0^t S_k(\tau)\tilde{r}(\tau)d\tau \\ &\quad - \frac{1}{2}\beta_2 S_{k-1}^2(t). \end{aligned} \tag{34}$$

Appendix B

The difference in the second Lyapunov function $V_k^2(t)$ between $k\text{th}$ and $(k-1)\text{th}$ iterations is shown as follows:

$$\Delta V_k^2(t) = \beta_1 |S_k(t)| - \beta_1 |S_{k-1}(t)|. \tag{35}$$

Differentiating $\beta_1|S_k(t)|$ with respect to time t yields

$$\frac{d}{dt}\left(\beta_1 |S_k(t)|\right) = \beta_1 \mathrm{sgn}(S_k)\dot{S}_k(t). \tag{36}$$

Based on (35) and (36), it follows that:

$$\Delta V_k^2(t) = \int_0^t \beta_1 \mathrm{sgn}(S_k)\dot{S}_k(\tau)d\tau - \beta_1 |S_{k-1}(t)|. \tag{37}$$

Combining (16) and (21) into (37) yields

$$\begin{aligned}\Delta V_k^2(t) &= \beta_1 \int_0^t \mathrm{sgn}(S_k)\phi_k(\tau)d\tau - \beta_1 |S_{k-1}(t)| \\ &\quad + \beta_1 \int_0^t \mathrm{sgn}(S_k)(-g\mathrm{sgn}(S_k) - \eta S_k(\tau) - \tilde{r}(\tau))d\tau \\ &= \beta_1 \int_0^t \mathrm{sgn}(S_k)\phi_k(\tau)d\tau - \beta_1 \int_0^t \eta\,|S_k(\tau)|\,d\tau \\ &\quad + \beta_1 \int_0^t \mathrm{sgn}(S_k)\left(-g\cdot \mathrm{sgn}(S_k) - \tilde{r}(\tau)\right)d\tau \\ &\quad - \beta_1 |S_{k-1}(t)|. \end{aligned} \tag{38}$$

APPENDIX C

The difference in the third Lyapunov function $V_k^3(t)$ between kth and $(k-1)$th iterations can be expressed as

$$\Delta V_k^3(t) = \frac{1}{2q}\int_0^t \left(\phi_k^T(\tau)\phi_k(\tau) - \phi_{k-1}^T(\tau)\phi_{k-1}(\tau)\right)d\tau. \tag{39}$$

In reference to the relationship $(a-b)^T(a-b) - (a-c)^T(a-c) = (c-b)^T(2(a-b)+(b-c))$, the relationship in (39) also holds

$$\begin{aligned}
&\frac{1}{2q}\left(\phi_k^T\phi_k - \phi_{k-1}^T\phi_{k-1}\right)\\
&= \frac{1}{2q}(\hat{f}_{k-1}-\hat{f}_k)\left(2(f_k-\hat{f}_k)+(\hat{f}_k-\hat{f}_{k-1})\right)\\
&= \frac{1}{2q}(\hat{f}_k-\hat{f}_{k-1})(\hat{f}_k-\hat{f}_{k-1}-2f_k)\\
&= \frac{1}{q}(\hat{f}_k-f_k)(\hat{f}_k-\hat{f}_{k-1}) - \frac{1}{2q}(\hat{f}_k-\hat{f}_{k-1})(\hat{f}_k-\hat{f}_{k-1}).
\end{aligned} \tag{40}$$

According to the update law (15), the above-mentioned equation can be expanded as

$$\begin{aligned}
&\frac{1}{2q}\left(\phi_k^T\phi_k - \phi_{k-1}^T\phi_{k-1}\right)\\
&= \frac{1}{q}\phi_k\left(-q\left(\beta_1\mathrm{sgn}(S_k)+\beta_2 S_k(t)\right)\right)\\
&- \frac{q}{2}(\beta_1\mathrm{sgn}(S_k)+\beta_2 S_k(t))^2.
\end{aligned} \tag{41}$$

Therefore, $V_k^3(t)$ is related to sliding surface dynamics in the following manner:

$$\begin{aligned}
\Delta V_k^3(t) = &-\frac{q}{2}\int_0^t \left(\beta_1\mathrm{sgn}(S_k)+\beta_2 S_k(\tau)\right)^2 d\tau\\
&- \beta_1\int_0^t \mathrm{sgn}(S_k)\phi_k(\tau)d\tau - \beta_2\int_0^t S_k(\tau)\phi_k(\tau)d\tau.
\end{aligned} \tag{42}$$

APPENDIX D

The difference in the fourth Lyapunov function $V_k^4(t)$ between kth and $(k-1)$th iterations has the following form:

$$\Delta V_k^4(t) = \frac{1}{2\gamma}\beta_2\tilde{r}_k^2(t) - \frac{1}{2\gamma}\beta_2\tilde{r}_{k-1}^2(t). \tag{43}$$

Differentiating $\beta_2\tilde{r}_k^2(t)$ with respect to time t yields

$$\frac{d}{dt}\left(\beta_2\tilde{r}_k^2(t)\right) = 2\beta_2\tilde{r}_k(t)\dot{\tilde{r}}_k(t). \tag{44}$$

Based on (20) and (44), (43) has an alternative form

$$\begin{aligned}
\Delta V_k^4(t) &= \int_0^t \frac{1}{\gamma}\beta_2\tilde{r}_k(\tau)\dot{\tilde{r}}_k(\tau)d\tau - \frac{1}{2\gamma}\beta_2\tilde{r}_{k-1}^2(t)\\
&= \int_0^t \frac{1}{\gamma}\beta_2\tilde{r}_k(\tau)\left(\gamma S_k(\tau) - \dot{r}_k(\tau)\right)d\tau - \frac{1}{2\gamma}\beta_2\tilde{r}_{k-1}^2(t).
\end{aligned} \tag{45}$$

The system disturbance is considered to vary much slowly compared to the system state, and $r(t)$ is defined as $\dot{r}(t)=0$; thus, (45) can be rearranged as

$$\Delta V_k^4(t) = \beta_2\int_0^t S_k(\tau)\tilde{r}_k(\tau)d\tau - \frac{1}{2\gamma}\beta_2\tilde{r}_{k-1}^2(t). \tag{46}$$

REFERENCES

[1] W. Qian, S. K. Panda, and J.-X. Xu, "Torque ripple minimization in PM synchronous motors using iterative learning control," *IEEE Trans. Power Electron.*, vol. 19, no. 2, pp. 272–279, Mar. 2004.

[2] J. A. Güemes, A. A. Iraolagoitia, J. J. Del Hoyo, and P. Fernández, "Torque analysis in permanent-magnet synchronous motors: A comparative study," *IEEE Trans. Energy Convers.*, vol. 26, no. 1, pp. 55–63, Feb. 2011.

[3] A. Gebregergis, M. Chowdhury, M. Islam, and T. Sebastian, "Modeling of permanent magnet synchronous machine including torque ripple effects," *IEEE Trans. Ind. Appl.*, vol. 51, no. 1, pp. 232–239, Jan. 2015.

[4] N. Nakao and K. Akatsu, "Suppressing pulsating torques: Torque ripple control for synchronous motors," *IEEE Ind. Appl. Mag.*, vol. 20, no. 6, pp. 33–44, Sep. 2014.

[5] J. Y. Hung and Z. Ding, "Design of currents to reduce torque ripple in brushless permanent magnet motors," *Proc. Inst. Electr. Eng. B*, vol. 140, no. 4, pp. 260–266, Jul. 1993.

[6] D. C. Hanselman, "Minimum torque ripple, maximum efficiency excitation of brushless permanent magnet motors," *IEEE Trans. Ind. Electron.*, vol. 41, no. 3, pp. 292–300, Jun. 1994.

[7] T. Liu, "Parameter, speed, position estimations and torque ripple minimization in permanent magnet synchronous motor," Univ. Akron, Akron, OH, USA, 1999.

[8] V. Petrovic, R. Ortega, and A. M. Stankovic, "Design and Implementation of an adaptive controller for torque ripple minimization in PM synchronous motors," *IEEE Trans. Power Electron.*, vol. 15, no. 5, pp. 871–880, Sep. 2000.

[9] P. Mattavelli, L. Tubiana, and M. Zigliotto, "Torque-ripple reduction in PM synchronous motor drives using repetitive current control," *IEEE Trans. Power Electron.*, vol. 20, no. 6, pp. 1423–1431, Nov. 2005.

[10] K. Basu, J. S. S. Prasad, and G. Narayanan, "Minimization of torque ripple in PWM ac drives," *IEEE Trans. Ind. Electron.*, vol. 56, no. 2, pp. 553–558, Feb. 2009.

[11] H. Zhu, X. Xiao, and Y. Li, "Torque ripple reduction of the torque predictive control scheme for permanent magnet synchronous motors," *IEEE Trans. Ind. Electron.*, vol. 59, no. 2, pp. 871–877, Feb. 2012.

[12] Y. Yuan, F. Auger, and L. Loron, "Torque ripple reduction in permanent magnet synchronous machine using angle-based iterative learning control," in *Proc. 38th Annu. Conf. IEEE Ind. Electron. Soc.*, Montreal, QC, Oct. 2012, pp. 2518–2523.

[13] K. Jezernik, J. Korelic, and R. Horvat, "PMSM sliding mode FPGA-based control for torque ripple reduction," *IEEE Trans. Power Electron.*, vol. 28, no. 7, pp. 3549–3556, Jul. 2013.

[14] Y. Xu, N. Parspour, and U. Vollmer, "Torque ripple minimization using online estimation of the stator resistances with consideration of magnetic saturation," *IEEE Trans. Ind. Electron.*, vol. 61, no. 9, pp. 5105–5114, Sep. 2013.

[15] S. Chai, L. Wang, and E. Rogers, "A cascade MPC control structure for a PMSM with speed ripple minimization," *IEEE Trans. Ind. Electron.*, vol. 60, no. 8, pp. 2978–2987, Aug. 2013.

[16] D. Flieller, N. K. Nguyen, and P. Wira, "A self-learning solution for torque ripple reduction for nonsinsoidal permanent magnet motor drives based on artificial neural networks," *IEEE Trans. Ind. Electron.*, vol. 61, no. 2, pp. 655–666, Feb. 2014.

[17] Y. Cho, K. Lee, J. Song, and Y. I. Lee, "Torque-ripple minimization and fast dynamic scheme for torque predictive control of permanent-magnet synchronous motors," *IEEE Trans. Power Electron.*, vol. 30, no. 4, pp. 2182–2190, Apr. 2015.

[18] Q. Liu and K. Hameyer, "Torque ripple minimization for direct torque control of PMSM with modified FCSMPC," *IEEE Trans. Ind. Appl.*, vol. 52, no. 6, pp. 4855–4864, Nov. 2016.

[19] Z. Zeng, C. Zhu, and X. Jin, "Hybrid space vector modulation strategy for torque ripple minimization in three-phase four-switch inverter-fed PMSM drives," *IEEE Trans. Ind. Electron.*, vol. 64, no. 3, pp. 2122–2134, Mar. 2017.

[20] Y. A.-R. I. Mohamed, "A newly designed instantaneous-torque control of direct-drive PMSM servo actuator with improved torque estimation and control characteristics," *IEEE Trans. Ind. Electron.*, vol. 54, no. 5, pp. 2864–2873, Oct. 2007.

[21] Y. Cho, K.-B. Lee, and J.-H. Song, "Torque ripple minimization and fast dynamic scheme for torque predictive control of permanent magnet synchronous motors," *IEEE Trans. Power Electron.*, vol. 30, no. 4, pp. 1358–1365, Apr. 2015.
[22] Y. Ren and Z. Q. Zhu, "Reduction of both harmonic current and torque ripple for dual three-phase permanent magnet synchronous machine using modified switching-table-based direct torque control," *IEEE Trans. Ind. Electron.*, vol. 62, no. 11, pp. 6671–683, Nov. 2015.
[23] Z. Bien and J.-X. Xu, *Iterative Learning Control-Analysis, Design, Integration and Applications*. New York, NY, USA: Springer, 2012.
[24] B. H. Lam, S. K. Panda, and J. X. Xu, "Reduction of periodic speed ripples in PM synchronous motors using iterative learning control," in *Proc. 26th Annu. Conf. IEEE Ind. Electron. Soc.*, Nagoya, Aichi, Japan, Oct. 2000, pp. 1406–1411.
[25] W. Qian, S. K. Panda, and J. Xu, "Speed ripple minimization in PM synchronous motor using iterative learning control," *IEEE Trans. Energy Convers.*, vol. 20, no. 1, pp. 53–61, Mar. 2005.
[26] J. Xu, S. K. Panda, Y. Pan, T. Lee, and B. H. Lam, "A modular control scheme for PMSM speed control with pulsating torque minimization," *IEEE Trans. Ind. Electron.*, vol. 51, no. 3, pp. 526–536, Jun. 2014.
[27] H. Shang, L. Zhao, and T. Wang, "Torque ripple reduction for permanent magnet synchronous motor based on learning control," in *Proc. 2nd Int. Conf. Inf. Sci. Control Eng.*, 2015, pp. 1001–1005.
[28] X. Zhang, L. Sun, and K. Zhao, "Nonlinear speed control for PMSM system using sliding mode control and disturbance compensation techniques," *IEEE Trans. Power Electron.*, vol. 28, no. 3, pp. 1358–1365, Mar. 2013.
[29] S. Li, M. Zhou, and X. Yu, "Design and implementation of terminal sliding mode control method for PMSM speed regulation system," *IEEE Trans. Ind. Informat.*, vol. 9, no. 4, pp. 1879–1891, Nov. 2013.
[30] L. Zhu, S. Z. Jiang, Z. Q. Zhu, and C. C. Chan, "Analytical methods for minimizing cogging torque in permanent-magnet machines," *IEEE Trans. Magn.*, vol. 45, no. 4, pp. 2023–2031, Apr. 2009.

Jing Liu (S'16) was born in LiaoNing, China, in 1991. She received the B.E. degree in electrical engineering from the Nanjing University of Aeronautics and Astronautics, Nanjing, China, in 2013. She is currently working toward the Ph.D. degree in the Changchun Institute of Optics, Fine Mechanics and Physics, Chinese Academy of Sciences, Changchun, China.

Her research interests include electric machines and drives and high-precision machine control techniques.

Hongwen Li (M'16) was born in Sichuan, China, in 1970. He received the B.E. degree in electrical automation from Sichuan University of Science and Engineering, Zigong, China, in 1993, and the M.S. and Ph.D degrees in electrical engineering from Jinlin University of Technology, Changchun, China, in 1996 and 2007, respectively.

From 1996 to 2002, he was an Associate Professor with the Jinlin University of Technology. Since 2002, he has been in the Changchun Institute of Optics, Fine Mechanics, and Physics, Chinese Academy of Sciences, Changchun, China, where he is currently a Professor in the Department of Optical-Electronic Detection. He has authored/coauthored more than 50 publications in his main areas of research, which include optical-electric sensor technologies, switching-mode power supply techniques, electric machines and drives, and high-precision machine control techniques.

Yongting Deng (M'16) was born in Shandong, China, in 1987. He received the B.E. degree in electrical engineering from the China University of Petroleum, Beijing, China, and the M.S. and Ph.D. degrees from the Changchun Institute of Optics, Fine Mechanics and Physics, Chinese Academy of Sciences, Changchun, China, in 2015.

He is currently an Associate Professor in the Changchun Institute of Optics, Fine Mechanics and Physics, Chinese Academy of Sciences. His research interests include controller design for ac motor drives and linear motor drives, intelligent control, and digital control using the DSP and FPGA implementations.